



# Influence of welding parameters and surface preparation on thin copper–copper sheets welded by ultrasonic welding process

Rafael Nunes<sup>1</sup> · Koen Faes<sup>1</sup> · Sylvia De Meester<sup>2</sup> · Wim De Waele<sup>2</sup> · Andrzej Kubit<sup>3</sup>

Received: 20 April 2022 / Accepted: 14 September 2022 / Published online: 28 September 2022  
© The Author(s) 2022

## Abstract

Ultrasonic welding is increasingly used in industry. In this paper, the influence of ultrasonic welding parameters (USW) on the joint strength and quality was analysed. The properties of the USW joints depend on many factors. The work focuses on the influence of the technological parameters and the surface properties of welded EN Cu-ETP copper sheets with a thickness of 1 mm. The impact of the process parameters, such as welding time, pressure, vibration amplitude and the surface roughness on the lap shear strength and the metallographic weld properties was analysed. The welding energy for each variant was also determined. The research was conducted on the basis of a full factorial design of experiments. The optimal process parameters were determined to obtain high-quality joints in terms of strength and weld quality. Based on the presented experimental study, it was demonstrated that the ultrasonic vibration amplitude has the greatest impact on the joint strength. A surface preparation with acetone resulted in the highest tensile strength and welding energy and, making any additional surface treatment prior to welding unnecessary.

**Keywords** Ultrasonic welding · Parameter optimisation · Surface treatment · Tensile strength

## 1 Introduction

The ultrasonic welding technology (USW) is well known and is now widely used for joining polymer materials. Recently, it has been increasingly used in industrial applications for joining metals. This is due to the increasing demand for ecological solutions in transport, involving that vehicles must be lighter in order to consume less energy, which results from international standards and regulations on the reduction of greenhouse gas emissions [1]. This translates into the need to join different metals with each other, and the joining technology must not require significant labour and energy consumption. Due to the growing use of electric cars in transport, the Cu-Cu homogeneous welds are very important in the context of the production of battery

sets [2–7]. In case of joints of copper elements constituting electrical circuits, the electrical conductivity and strength of the joint are important [8]. Not only is the static strength important, but especially the fatigue and dynamic strength, since the joints are exposed to these loads during operation [3, 4, 7–9].

Joining of highly conductive and reflective metals has always been very challenging with fusion welding techniques, such as arc, laser and electron beam welding processes [6–14]. Conventional welding technologies operating above the melting point of the metals to be joined often cause metallurgical defects, such as the formation of brittle intermetallic compounds, brittle phases and porosity in the fusion zone, as a result of the solidification [15–20]. The solutions to these problems are welding technologies that occur below the melting point of the metals to be joined, in the solid phase.

One such technology is ultrasonic welding (USW). USW is a friction-based welding technology which may be widely used in the future for the construction of electric car power supply systems, due to its specific advantages [9, 21, 22]. The USW technology is based on the phenomenon of interfacial friction, as a result of which metals are joined by diffusion and adhesion of softened metals [3, 23]. Due to this

✉ Andrzej Kubit  
akubit@prz.edu.pl

<sup>1</sup> Belgian Welding Institute, Zwijnaarde, Belgium

<sup>2</sup> Department of Electromechanical, Systems and Metal Engineering, Ghent University, Ghent, Belgium

<sup>3</sup> Department of Manufacturing and Production Engineering, Rzeszow University of Technology, Rzeszow, Poland

joining mechanism, the structure of USW welds is usually free of brittle intermetallic layers along the weld interface, which ensures lower electrical resistance [9, 24, 25]. Therefore, the USW welding technology is suitable for joining metals used in electrical engineering, such as silver, copper, gold and aluminium [26].

In general, the USW welding process is based on the fact that the element generating ultrasonic vibrations, i.e. the piezoelectric transducer, converts electrical energy into the vibration of a sonotrode. This results in local heat generation due to frictional forces, which results into material softening [27, 28]. Ultrasonic vibrations and pressure cause diffusion in the joined materials and, as a result, their joining due to adhesion [26]. Importantly, ultrasonic vibrations have the additional advantage that they break the oxide layer on the surfaces of the metals to be joined [29, 30]. Gencsoy et al. [31] described in detail the mechanisms that take place during joining of materials using the USW method. These are mainly interfacial diffusion, adhesion by plastic deformation, local heating and mechanical interlocking.

Also important to mention is that USW is a technology that works well for joining unweldable metals, as well as for dissimilar joints, i.e. metals with other materials such as ceramics and glass [32–36].

Although there are many studies evaluating the result and quality of joints realised by USW, there is a lack of information on how the samples should be prepared in order to achieve optimized values of the tensile strength.

In this study, the authors propose a strategy for parametrisation of the USW process applied to Cu-Cu thin sheets, followed by the evaluation of the influence of each parameter and their combinations on the welding energy and the joint tensile strength. Besides that, eight different treatments resulting in eight different surface roughness were evaluated.

## 2 Materials and methods

Investigations of the influence of the parameters of the USW welding process on the joint properties were carried out for overlap joints with the dimensions shown in Fig. 1. Joints of EN Cu-ETP (Electrolytic Tough Pitch) copper sheets were analysed. This material is commonly used in electrotechnical applications due to its very good electrical conductivity. The considered material is characterized by a good ductility and plasticity, and is resistant to corrosion. The sheets used in the tests were 1 mm thick and have a copper content of 99,971%.

The research was performed using the Telsonic MPX Ultrasonics Linear Metal Welding Press equipment. The specifications of this machine are a nominal power of 3.6 kW, a frequency of 20 kHz, the maximum load that can be applied is 1600 N and the maximum vibration

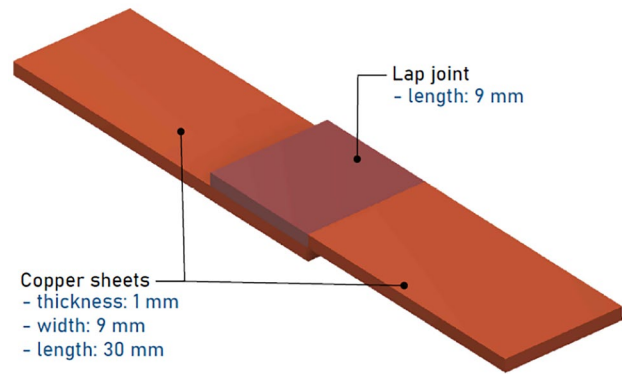


**Fig. 1** Configuration and dimensions of the overlap joint of copper sheets

amplitude is 66  $\mu\text{m}$ . The control software allows setting a vibration amplitude between 50 and 100% of this maximum value. The sonotrode moves horizontally back and forth, resulting in a tangential transfer of the waves into the workpieces. The parameters of the device enable welding of both ferritic and non-ferritic metal alloys.

In this work, the influence of three parameters, i.e. welding time, pressure and amplitude, on the joint properties was investigated. Various values of these parameters were considered according to the established design of the experiment.

The other process parameters were kept constant for all welding trials. The trigger time is set equal to 0.04 s, and the pressure build up time to 0.30 s. This means that the sonotrode starts to vibrate after 0.04 s until it reaches the required pressure after 0.30 s. During the experiments, the hold function is used to keep the welded sheets together after the weld cycle. The hold time and pressure are chosen equal to the selected time and pressure during the weld cycle.

The quantification of the surface roughness [37] was performed with a device that uses a tactile probe moving over the surface to measure the asperities and roughness peaks. The device performs  $n$  measurements during the inwards movement of the probe and returns the average values of  $R_a$  and  $R_z$ .  $R_a$  is the average roughness of the surface.  $R_z$  is the difference between the highest “peak” and the deepest “valley” of the surface.

Besides destructive testing, the weld properties were assessed based on metallographic analysis. The research was carried out using an optical microscope. The metallographic specimens were made in a plane parallel to the direction of the sonotrode vibrations. The metallographic analysis was divided into two stages. In the first preliminary stage, observations were made on a macroscopic scale; the purpose of which was to determine the length

of the resulting joint, as well as to indicate defects in the joint. Selected areas were subjected to an additional, more detailed analysis at higher magnifications by etching the samples with a 10% ammonia solution in water saturated with hydrogen peroxide. The etching time was 20 s.

Based on experimental preliminary tests, the extreme values of the welding parameters were determined. The following ranges of parameters were adopted: the welding time was varied in the range of 1.5–4.0 s, the pressure in the range of 2.0–5.0 bar and the amplitude in the range of 50–90%.

As part of the preliminary research, samples were evaluated through visual and peel test examinations and classified into three levels based on the peel test results. In order to allow a quantitative comparison, the scoring of the welds was done according to levels 1, 3 and 5 according to the failure variants presented in Fig. 2.

After conducting preliminary investigations and after determining the boundary values of the process parameters, a full factorial design of experiments (DoE) was created. According to the adopted plan, the process parameters were set at three levels; as a result, 27 combinations of parameters were obtained. The complete research plan is presented as a design space of a 3-factor 3-level full factorial DoE (Fig. 3). Detailed values of welding parameters according to the adopted experimental plan are listed in Table 1. Four welds were created for each parameter combination; three of them were intended for lap shear tests, and one for metallographic analysis.

The static strength tests were carried out in accordance with the requirements defined by the EN ISO 14273 standard [38]. Lap shear tests were performed using a universal testing machine. A constant displacement rate of 2 mm/min was used during the tests. The tensile test machine contains 2 wedge-action grips, which clamp both sides of the welded test specimens. No other supports were used during testing. By using spacer plates, a shear load is imposed on the weld, thereby preventing peel stresses.

For each of the four samples welded using a given parameter combination of the research plan, the welding

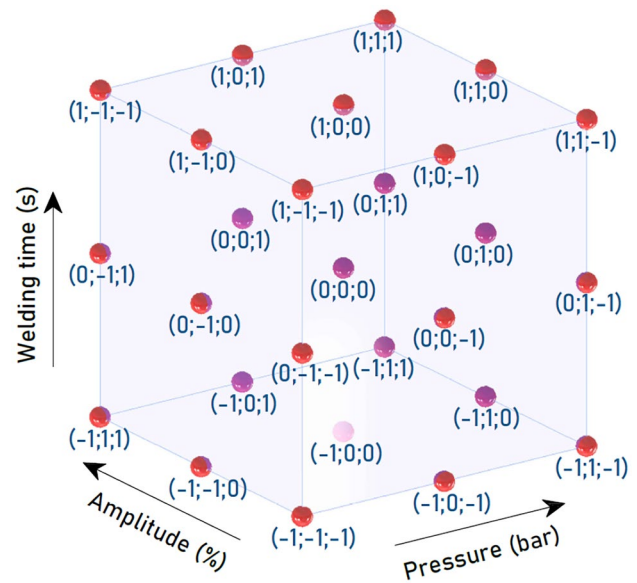


Fig. 3 DoE matrix used in the investigations

energy was measured, while three samples were subjected to the lap shear test. Based on the obtained test results, the average value and the standard deviation were determined.

### 3 Results and discussion

#### 3.1 Influence of the welding parameters on the welding energy

One of the basic criteria for selecting welding parameters is the minimization of the process energy. The energy of ultrasonic welding strictly depends on the three parameters considered, but also on the efficiency of the welding equipment, including its energy dissipation coefficient. For each of the parameter levels, the welding energy value was read directly from the welding machine at each of the four repetitions, marked as A, B, C and D. Average values and standard deviations of the welding energy with the given parameters were determined. The results are summarized in Table 2.

After the measurements of the welding energy, the regression equation (Eq. 1) was determined, which defines

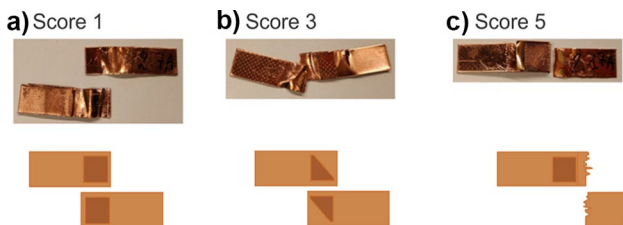


Fig. 2 Peel testing classification based on the type of joint failure, following the criteria for a low, b intermediate and c high weld quality

Table 1 Welding parameters used in the DoE matrix

DoE Level	Welding time (s)	Pressure (bar)	Vibration amplitude (%)
-1	1.50	2.0	50
0	2.75	3.5	70
1	4.00	5.0	90

**Table 2** Standardized effects of the welding parameters on the welding energy

Weld time (s)	Pressure (bar)	Amplitude (%)	Energy A (J)	Energy B (J)	Energy C (J)	Energy D (J)	Energy AVG (J)	Energy std dev (J)
1.50	2	50	693.2	841.3	951	894	844.9	111
1.50	2	70	1259	1341.7	1459.4	1417.9	1369.5	88
1.50	2	90	1509.2	1511	1530.7	1528.9	1520.0	11
1.50	3.5	50	1246.8	1241.2	1281.2	1224.5	1248.4	24
1.50	3.5	70	1688.2	1626.4	1721.6	1731.2	1691.9	47
1.50	3.5	90	2071.9	2168.7	2092.9	2343	2169.1	123
1.50	5	50	1313.7	1323.8	1301.8	1312.4	1312.9	9
1.50	5	70	2071.8	2038.5	1933.6	2112.7	2039.2	77
1.50	5	90	2785.3	2914.8	2632.1	2808.4	2785.2	117
2.75	2	50	1447.8	1541.9	1466	1575.1	1507.7	61
2.75	2	70	2299.8	2212.5	2177.1	2194.2	2220.9	55
2.75	2	90	2499.5	2578.3	2475	2559.7	2528.1	49
2.75	3.5	50	2202.7	2152.8	2219.5	2168.8	2186.0	31
2.75	3.5	70	2947.9	3048.3	2984.5	3217	3049.4	119
2.75	3.5	90	4081.7	3978.5	3996.2	4030.2	4021.7	45
2.75	5	50	2543.3	2494.5	2381.2	2356.7	2443.9	89
2.75	5	70	3613.9	3646.1	3533.9	3978.5	3693.1	196
2.75	5	90	4898.8	5150.4	5302.4	5335.3	5171.7	199
4.00	2	50	2396.6	2376.3	2396.1	2272.7	2360.4	59
4.00	2	70	3132.3	3194.6	3244.7	3135.1	3176.7	54
4.00	2	90	3636.2	3965.3	4063.4	3907	3893.0	183
4.00	3.5	50	3356.3	3498.4	3242.7	3457.5	3388.7	114
4.00	3.5	70	4261	4705.2	4240.7	4861.2	4517.0	314
4.00	3.5	90	5835.4	5920.9	6097.7	5917.8	5943.0	111
4.00	5	50	3284.7	3564.2	3451.3	3661.4	3490.4	162
4.00	5	70	5168.3	5814.6	5920.7	6068.2	5743.0	397
4.00	5	90	6657	5753.8	6686.3	6014.7	6278.0	467

the relationship between the parameters and the average energy value. A Pareto diagram (Fig. 4) was also created in order to determine the correlation between the individual parameters and their influence on the measurement results.

$$E = 847 - 28 WT - 3.85 P - 13.6 A + 57 \times P + 7.35 WT \times A + 6.25 P \times A + 1.53 WT \times P \times A \quad (1)$$

where  $E$  is the average energy (J),  $WT$  is the welding time (s),  $P$  is the pressure (bar) and  $A$  is the amplitude (%).

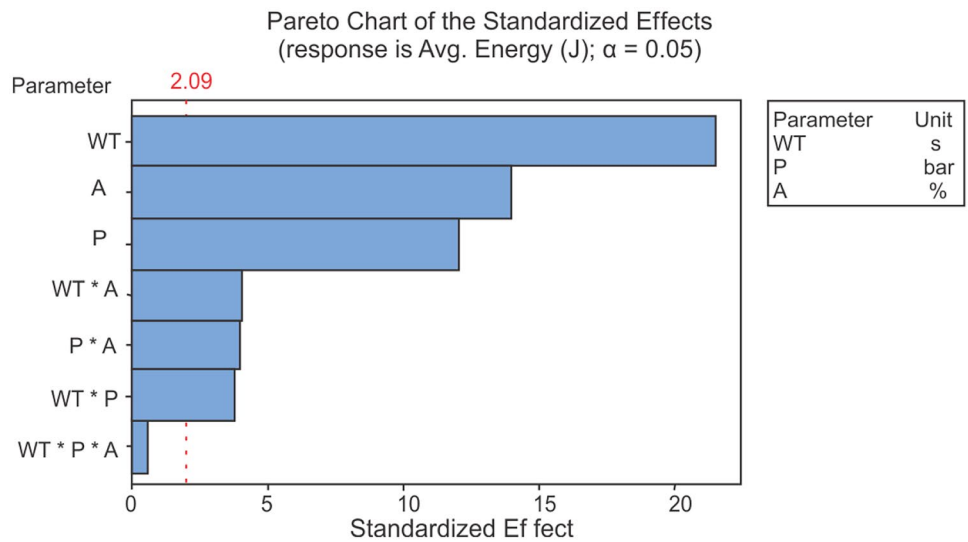
Based on the analysis, it can be observed that the welding time has the greatest impact on the welding energy from the three parameters under consideration.

The contour plots of the average energy as a function of the vibration amplitude and pressure for a constant welding time reveal an increase of the energy when one of the welding parameters is increased (Fig. 5).

### 3.2 Influence of the welding parameters on the lap shear strength

In addition to the welding energy, the second criterion taken into account when selecting the parameters is the joint quality, determined in first place based on the load bearing capacity. Table 3 presents the results of the lap shear tests for each parameter combination along with the average value and standard deviation. The individual samples were marked with B, C and D, while the samples marked with A were subjected to a metallographic investigation. The table also shows the failure modes according to which the samples failed. For each parameter combination, one peel test was performed. The failure mode where the joint failed in one of the sheet base materials (peel test score: 5) is considered the most advantageous failure mode. In this case, the weld nugget has a sufficient high strength. The other failure modes (peel test score: 1 and 3) resulted from non-optimised process parameters, yielding unwelded zones in the joint interface.

**Fig. 4** Pareto chart of the standardised effects of the welding parameters on the welding energy



For the value of the average load bearing capacity, the shear strength of the joint was determined, using a surface area of 9 mm<sup>2</sup>. As in case of the welding energy analysis, the correlation between the individual parameters and the

strength was also determined. For this purpose, the regression equation (Eq. 2) was determined and the Pareto diagram (Fig. 6) was created.

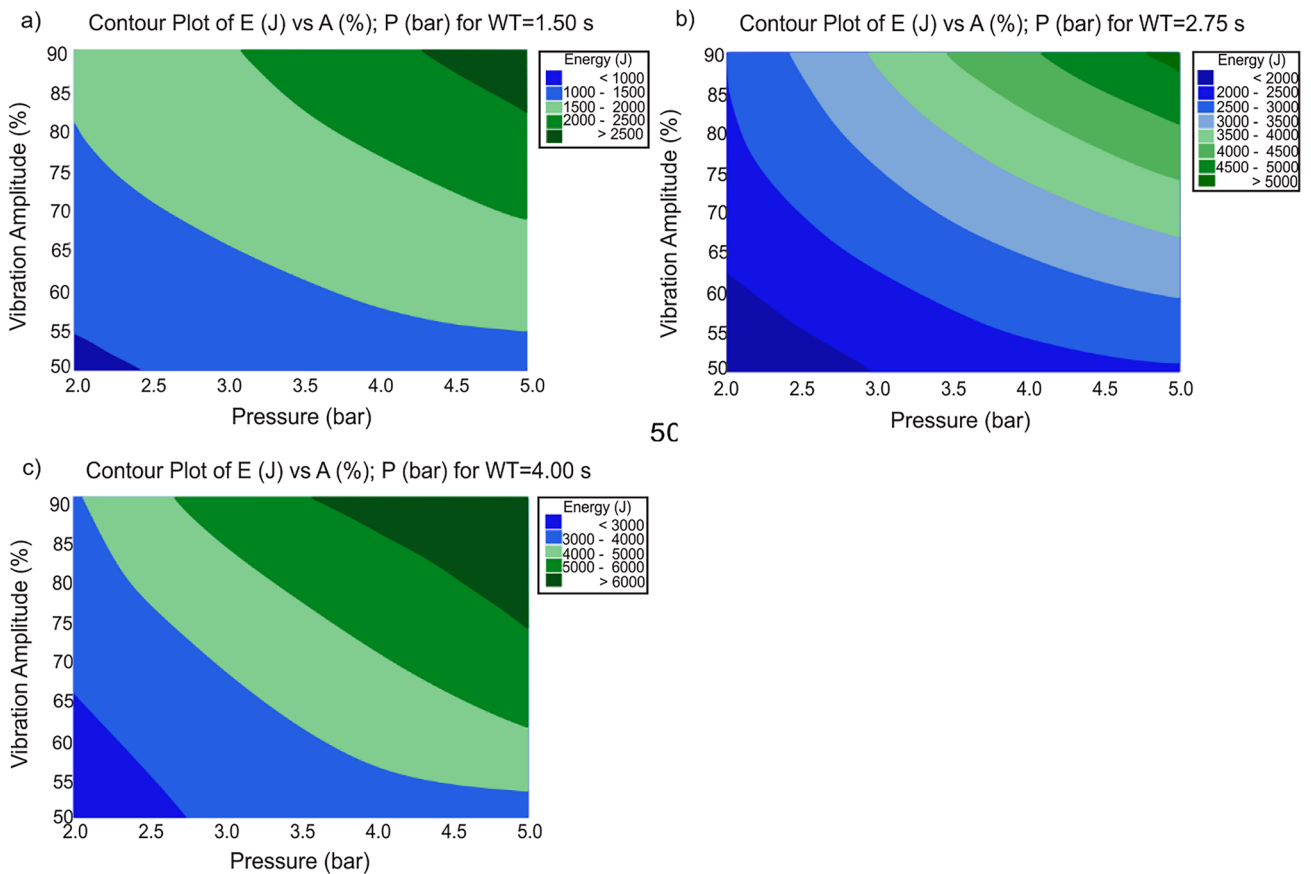


**Fig. 5** Contour plots of the energy vs vibration amplitude and pressure for a constant welding time

**Table 3** Standardized effects of the welding parameters on the welding energy

Weld time (s)	Pressure (bar)	Amplitude (%)	Peel test score	Tensile B (N)	Tensile C (N)	Tensile D (N)	Tensile AVG (N)	Tensile std dev (N)
1.50	2.0	50	1	1.83	2.21	1.45	1.83	0.38
1.50	2.0	70	5	2.23	2.25	1.85	2.11	0.23
1.50	2.0	90	5	2.23	2.22	2.22	2.22	0.00
1.50	3.5	50	5	2.30	2.25	2.31	2.29	0.03
1.50	3.5	70	5	2.27	2.28	2.25	2.26	0.02
1.50	3.5	90	5	2.80	2.08	1.80	2.23	0.52
1.50	5.0	50	5	2.28	2.32	2.31	2.30	0.02
1.50	5.0	70	5	2.32	2.30	2.23	2.28	0.05
1.50	5.0	90	5	1.52	2.05	1.66	1.75	0.27
2.75	2.0	50	5	2.16	2.24	2.30	2.23	0.07
2.75	2.0	70	5	2.20	2.09	2.18	2.16	0.06
2.75	2.0	90	5	2.04	2.14	2.05	2.08	0.06
2.75	3.5	50	5	2.27	2.28	2.28	2.28	0.00
2.75	3.5	70	5	2.08	2.20	1.96	2.08	0.12
2.75	3.5	90	5	1.29	1.27	0.93	1.16	0.20
2.75	5.0	50	5	2.26	2.28	2.21	2.25	0.04
2.75	5.0	70	5	2.24	2.27	2.07	2.19	0.11
2.75	5.0	90	5	1.11	0.75	0.75	0.87	0.21
4.00	2.0	50	5	2.26	2.20	2.20	2.22	0.03
4.00	2.0	70	5	2.13	2.09	2.09	2.10	0.03
4.00	2.0	90	5	1.78	1.77	1.88	1.81	0.06
4.00	3.5	50	5	2.23	2.24	2.24	2.23	0.00
4.00	3.5	70	5	1.74	2.12	1.60	1.82	0.27
4.00	3.5	90	5	0.88	0.53	0.61	0.67	0.19
4.00	5.0	50	5	2.22	2.30	2.24	2.25	0.04
4.00	5.0	70	5	1.72	1.68	1.38	1.59	0.18
4.00	5.0	90	5	0.52	0.58	0.55	0.55	0.03

$$\begin{aligned}
S = & -0.062 + 0.0706 WT + 0.0646 P + 0.00398 A \\
& - 0.0003 WT \times P - 0.000821 WT \times A - 0.000714 P \times A \\
& - 0.000130 WT \times P \times A
\end{aligned} \quad (2)$$

where  $S$  is the tensile strength ( $\text{kN}/\text{mm}^2$ ),  $WT$  is the welding time (s),  $P$  is the pressure (bar) and  $A$  is the vibration amplitude (%).

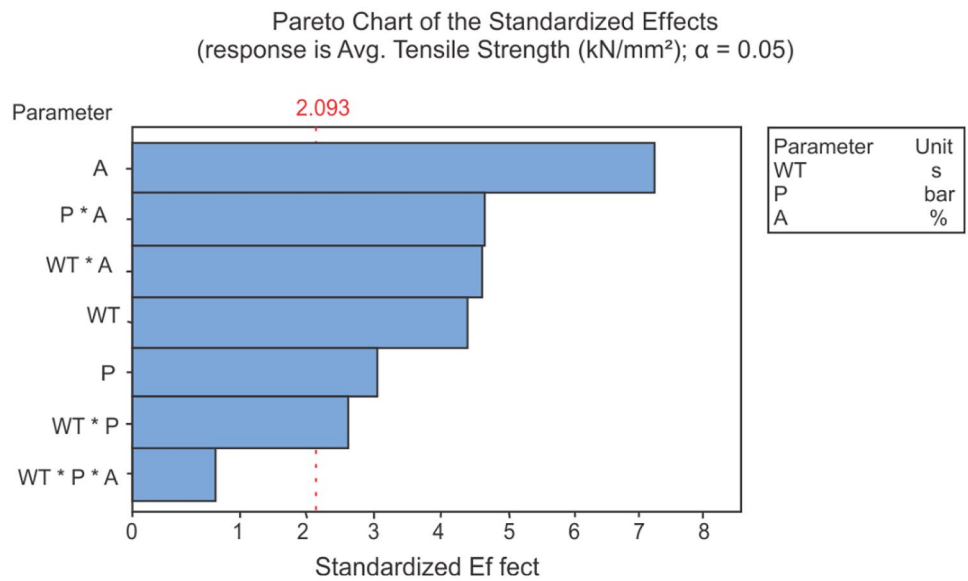
In the following results, the average tensile strength is represented as a percentage of the lap shear strength of the base material. The base material strength has been measured by performing a tensile test on three sheets with dimensions  $51 \times 9 \times 1.0$  mm and by calculating the average of the resulting forces at failure. The length of 51 mm corresponds to the average length of the welded samples, as each sheet is 30 mm long with an overlap of 9 mm (Fig. 1). The average measured force to break the copper base material equals 2.175 kN. The average lap shear strength of the copper sheets then corresponds to  $2.175 \text{ kN}/9.0 \text{ mm}^2 = 0.241 \text{ kN}/\text{mm}^2 = 241 \text{ MPa}$ .

The relation between the welding parameters and the tensile strength can be visualised using contour plots. Figure 7 shows the average relative tensile strength as a function of the pressure and vibration amplitude for a constant value of the welding time.

### 3.3 Relationship between welding energy and tensile strength

Considering the impact of the welding energy on the joint strength, it should be noted that, as with most welding technologies, a higher energy consumption results in a greater amount of heat generated during welding, which has an impact on the properties of the joint [39]. Too much heat generated in the weld area causes excessive plasticisation of the sheets to be welded, resulting in unwanted deformations and a large heat-affected zone. However, too little heat results into insufficient conditions for creation of a joint with

**Fig. 6** Pareto chart of the standardized effects of the welding parameters and their interactions on the average tensile strength



appropriate quality. Moreover, with the USW technique, an insufficient amount of heat generated leads to the formation of a joint with an insufficient surface area. Therefore, an optimal energy of the welding process is necessary, which

will enable the production of a high-strength joint free from structural defects.

Figure 8 shows a graph of the relationship between the relative lap shear strength and the welding energy, while

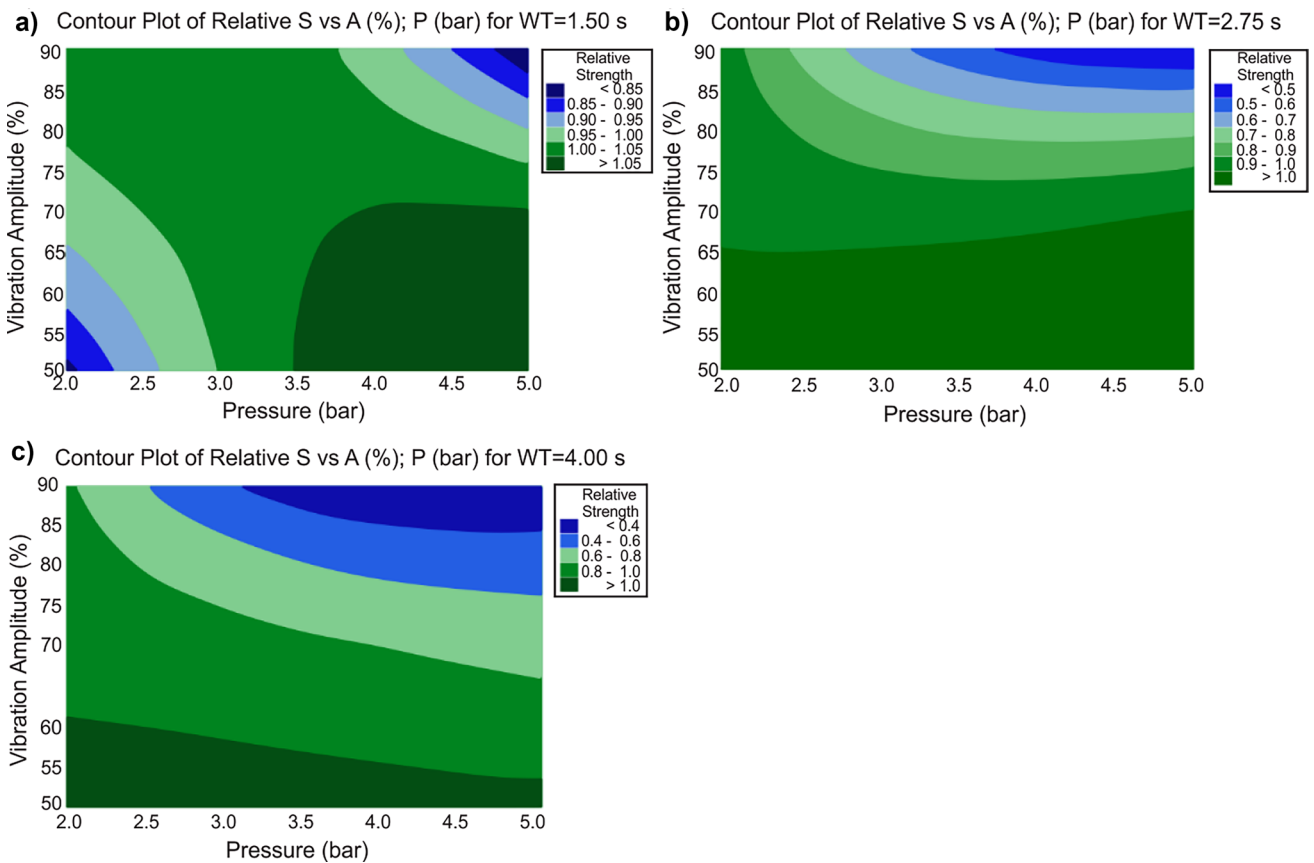


**Fig. 7** Contour plots of the relative average lap shear strength vs amplitude and pressure for a constant welding time: **a** 1.5 s; **b** 2.75 s; **c** 4 s

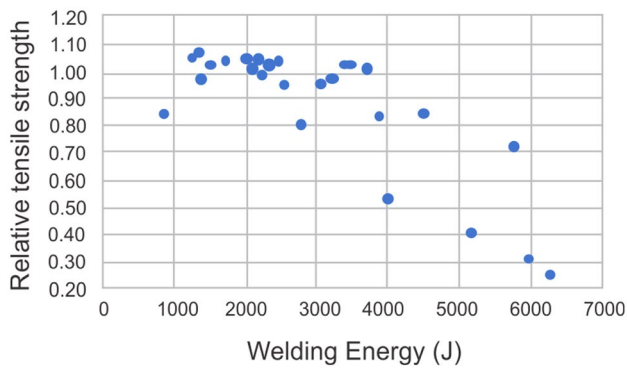


**Fig. 8** Relationship between the relative tensile strength as function of the welding energy

Table 4 summarises the relative lap shear strength values for all levels of the considered parameter combinations. It was observed that the highest strength values were obtained

**Table 4** Influence of the welding parameters on the relative tensile strength

Weld time (s)	Pressure (bar)	Amplitude (%)	Relative tensile strength
1.50	2.0	50	0.84
1.50	2.0	70	0.97
1.50	2.0	90	1.02
1.50	3.5	50	1.05
1.50	3.5	70	1.04
1.50	3.5	90	1.02
1.50	5.0	50	1.06
1.50	5.0	70	1.05
1.50	5.0	90	0.80
2.75	2.0	50	1.03
2.75	2.0	70	0.99
2.75	2.0	90	0.95
2.75	3.5	50	1.05
2.75	3.5	70	0.96
2.75	3.5	90	0.53
2.75	5.0	50	1.03
2.75	5.0	70	1.01
2.75	5.0	90	0.40
4.00	2.0	50	1.02
4.00	2.0	70	0.97
4.00	2.0	90	0.83
4.00	3.5	50	1.03
4.00	3.5	70	0.84
4.00	3.5	90	0.31
4.00	5.0	50	1.04
4.00	5.0	70	0.73
4.00	5.0	90	0.25

for the welding energy ranging from 1200 to 1300 J. Below 1000 J, the appropriate joint quality was not obtained, which proves that the welding energy is too low. Above 3800 J, there is a clear decrease in strength, which is attributed to the too high heat input, which results in excessive plasticisation of the joined specimens.

During the experimental research, some additional, macroscopic phenomena were observed, which took place as a result of increasing the values of the individual process parameters. These phenomena are listed in Table 5, mainly due to the high values of the welding time and pressure; the formation of a wavy surface in the joint area occurred. A too high pressure also resulted in elongation and deformation of the welded sheets due to deformation of the plasticised material in the area of the overlap.

### 3.4 Influence of the surface preparation

To investigate the influence of the surface roughness on the weldability of the Cu sheets, eight different surface conditions are investigated and compared. The surface preparation is applied on one side of the Cu sheets, where the sheets will be placed such that the treated surface touches each other during welding.

For each surface preparation, the average surface roughness is determined by performing three measurements in the longitudinal direction of the sheets and three measurements in the transversal direction. In this way, any directional influences of the surface preparations are characterised. This is particularly important for test pieces that have undergone rapid sanding with sandpaper, since the roughness in the direction of the grooves differs from the roughness in the perpendicular direction. Figure 9 shows examples of such sanded copper sheets. From these images, it is clear that the direction in which the roughness measurements are performed will have a big influence on the resulting roughness values. During the experiments, welds were made using sheets with grooves in several directions. Changing the direction of the grooves did not have an observable impact on the weldability of the sheets, parametrization of the process or the welding energy resulting from the process. In this way, it is expected that combination of the groove directions can be disregarded during the setup preparation. The roughness values corresponding with each surface preparation are given in Table 6.

When analysing the influence of the surface preparation on the joint properties, the following welding parameters were adopted, which were found to be appropriate on the basis of the previous tests. The value of the welding time was determined to be  $t = 1.5$  s, the pressure was equal to  $p = 5.00$  bar and the amplitude was set at the value of  $A = 70\%$ . This choice was made based on the



**Table 5** Effects of increasing parameter values on the weld interface

Parameter	Welding time	Pressure	Vibration amplitude
<b>Effects of increasing parameter value</b>	Increased welded area	Deformation and elongation of the sheets	The lowest influence
	Wavy surface	Wavy surface	

high weld strength resulting from this parameter combination. Moreover, the metallographic examination of this weld shows a large bonded area between the metal sheets (Fig. 10).

For each surface preparation, four repetitions were made to evaluate the influence on the welding energy and the lap shear strength. One of these welds is used to perform a metallographic examination of the weld interface. Any potential decrease of the metal sheets thickness as a result of the surface preparation is neglected during these experiments.

According to Silva et al. [40], degreasing the specimens with acetone is important to ensure a high amount of micro-welds or welded islands at the weld interface. The presence of oxides and contaminants on the surface can prevent a metal to metal contact and could hinder the weld formation. Although most oxides are broken down due to the ultrasonic welding process, it is still important to remove all contaminations from the surface. According to Harthoorn [17], light sanding of the surface of the workpieces can increase the amount of metal-to-metal contact and therefore have a positive influence on the size of the welded area. However, too high roughness values will result in mechanical interlocking or micro-welding of the asperities, which will hinder further movement of the

welding surfaces. Considering these observations, it is to be expected that a very high surface roughness will result in less qualitative welds, while a surface preparation resulting in a lightly sandpapered surface could be beneficial for the weld quality.

**3.4.1 Influence of the surface preparation on the welding energy**

During welding, the friction resulting from the ultrasonic waves will cause deformations of the surface asperities and will eventually create a joint between the sheets. A large amount of frictional energy is expected to be beneficial for the joint formation. However, too much friction at the weld interface will result in a high heat input which could be detrimental for the weld quality. Large amounts of heat cause deformations of the weld interface and will decrease the tensile strength of the welds.

Figure 11 shows the average energy values (four measurements per surface preparation) as a function of the Ra and Rz roughness measurements. Both graphs show a very similar behaviour; large roughness values result in a lower energy input, while lower roughness values can result in a very high welding energy. This is counterintuitive as a larger roughness usually results in more friction. In this case, the decrease of energy for a larger roughness value could be due to the formation of micro-welds at the locations of the surface asperities which will hinder further movement and friction at the weld interface, resulting in less welding energy. Harthoorn [17] observed a roughness limit above which it was nearly impossible to achieve a



**Fig. 9** Sanded copper sheets (500 mesh) with grooves in different directions

**Table 6** Roughness values for the different surface preparations

Surface preparation	Ra AVG (µm)	Rz AVG (µm)
1) Cleaning with acetone	0.18	1.43
2) Sandpaper: 80 mesh	1.93	13.55
3) Sandpaper: 180 mesh	1.21	8.49
4) Sandpaper: 500 mesh	0.54	4.31
5) Grinding	0.41	3.27
6) Rough milling	0.71	3.79
7) Finish milling	0.32	1.94
8) Etching (NH <sub>3</sub> + H <sub>2</sub> O <sub>2</sub> )	0.14	1.29

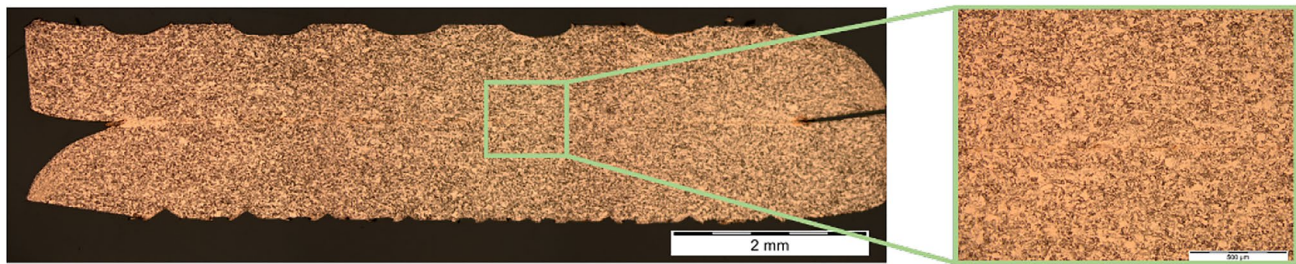


**Fig. 10** Metallographic cross section of the weld executed with the process parameters selected for surface preparation impact studies

weld. According to this publication, the reason for this is mechanical interlocking of the rough contact areas which hinders the relative movement of the surfaces to be welded.

The surface preparation corresponding with the highest welding energy observed in the experiments is a simple cleaning of the surfaces with acetone. This leads to the conclusion that there is no need for an elaborate surface preparation to obtain a higher welding energy.

### 3.4.2 Influence of the surface preparation on the tensile strength

In Fig. 12, the relative average lap shear strength (three measurements for each surface preparation) is shown as a function of the roughness value. In general, the same trend as for the welding energy can be observed; i.e. the welded specimens with the lowest surface roughness result in the highest values of the lap shear strength. However, the specimens sanded with a 180 mesh also results in a large lap shear strength. The only surface preparation resulting in a weld strength above the average base metal strength is cleaning of the surface with acetone. These results again confirm the previous observation that there is no added value in applying a surface pre-treatment to the workpieces before welding.

### 3.4.3 Metallographic examination

To evaluate the weld quality based on the amount of welded area and potential weld flaws, metallographic images are

made for one weld for each surface treatment. Figure 13 shows the etched cross sections of the welded samples prepared with all surface treatments. It is clear that sanding the workpieces with an 80 mesh sandpaper results in a large unwelded area as the black line on the right side of the image indicates a gap between the sheets. Sandpaper with a finer mesh gives a larger welded area.

The highest joint strength was obtained for the surfaces which were cleaned with acetone. Figure 14a shows the macrostructural view of the joint, i.e. a polished metallographic specimen. On the basis of this view, it can be observed that there is metallic continuity on the entire surface of the lap joint, which demonstrates a high joint quality. Figure 14b shows the macroscopic view of the etched sample that allows the microstructure of the weld to be assessed. It can be seen that welded islands have formed evenly along the joint (Fig. 14c, d).

The joints of the sheets, the surfaces of which were prepared with 180 and 500 sandpaper, are fully welded; however, the mentioned phenomenon of the formation of welded islands was observed on their interfaces. The observations showed that the smaller the sandpaper gradation, the smaller the welded islands are. Figure 15 shows a microscopic magnification of the weld interface for sheets prepared with 180 grit sandpaper. It can be observed here that the largest welded islands were formed at the leading edge of the joint, while in the middle of the joint, welded islands are much smaller. However, in case of joining sheets prepared with 500 grit sandpaper, the welded island phenomenon is minimal (Fig. 16).

**Fig. 11** Welding energy versus surface roughness

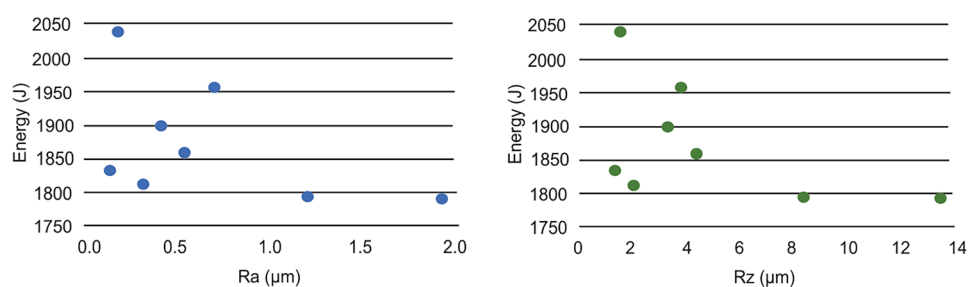
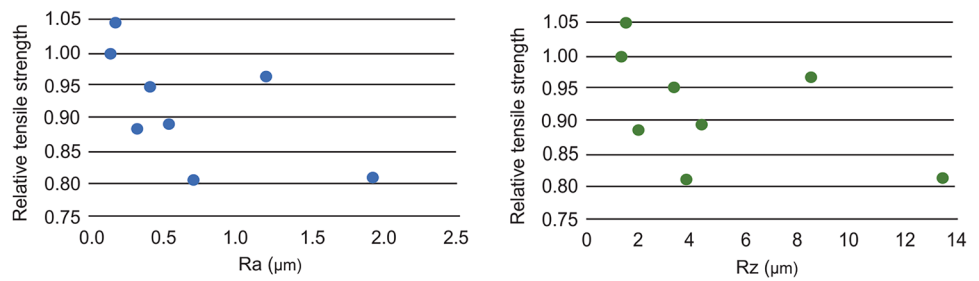


**Fig. 12** Surface roughness vs relative lap shear strength



These observations lead to the conclusion that when using sandpaper to increase the surface roughness of the workpieces, the use of a coarse grit will result in a weld with a smaller welded surface. An explanation for this may be the occurrence of mechanical interlocking or micro-welding of the surface asperities which hinders the further relative movement of the sheets and stops the welding process as described in [40, 41, 42].

Sandpaper with a finer mesh results in a larger welded area. However, the size of the welded islands decreases when a very fine mesh is used. This is in accordance with the research of Harthoorn [17], where light sanding of the surface led to an increased size of the welded area due to increased metal-to-metal contact.

The grinded specimen shows an elongation of the top workpiece which could be the result of a larger amount of heat input caused by friction at the interface. The weld

interface of this sample shows a large number of discontinuities in between the welded islands. These discontinuities are clearly visible on the polished cross-section of the weld (Fig. 17) and on the detailed images of the etched surface in Fig. 17b. This shows that grinding is not an efficient surface preparation for obtaining a weld with optimal quality.

Both milling processes (rough and finish) show a dark line at the interface of the etched weld samples in Fig. 14, which could point to an unwelded region. However, these lines are most likely a side-effect of the etching process, as no gaps are observed in the polished unetched cross sections (Fig. 18: rough milling and Fig. 19: finish milling). When examining the weld interface of the milled welds in closer detail, the welded islands appear in a much darker colour than for all other surface preparations. This is proving that the dark line visible in Fig. 13 does not correspond with a gap.

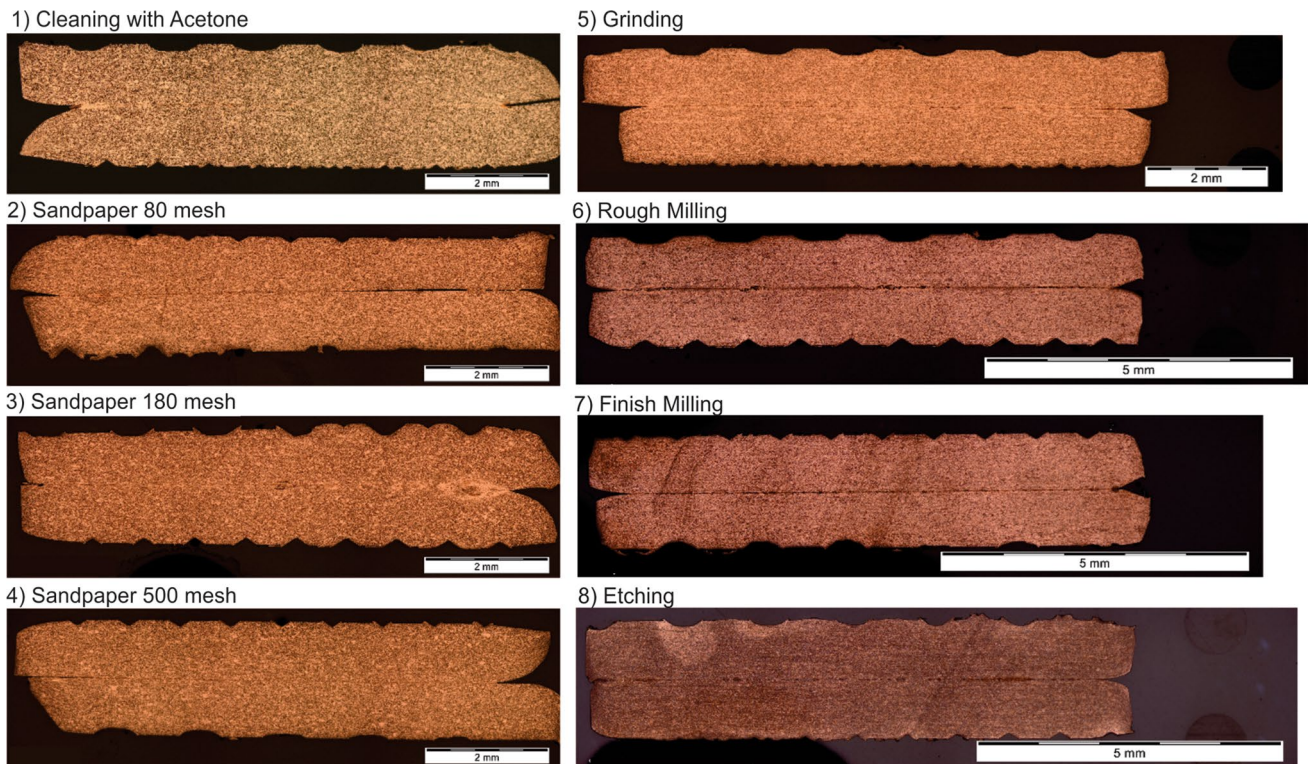


**Fig. 13** Metallographic images of the etched weld cross-sections for each surface treatment

**Fig. 14** Sample prepared with acetone: **a** macroscopic image of a polished Cu – Cu weld with  $t = 1.0$  mm ( $\times 50$ ); **b** etched ( $\times 50$ ); **c** and **d** detail images of the weld interface ( $\times 200$ )

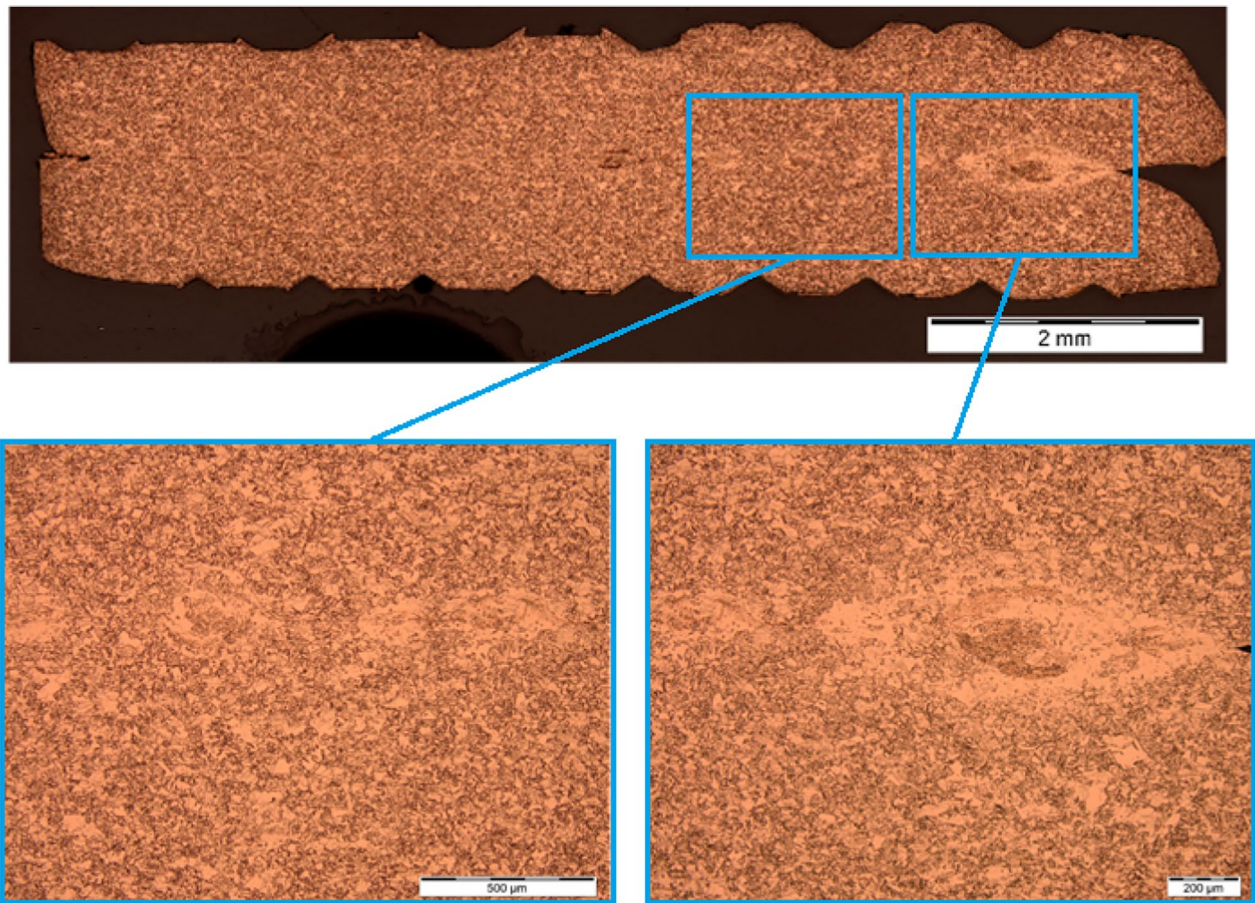
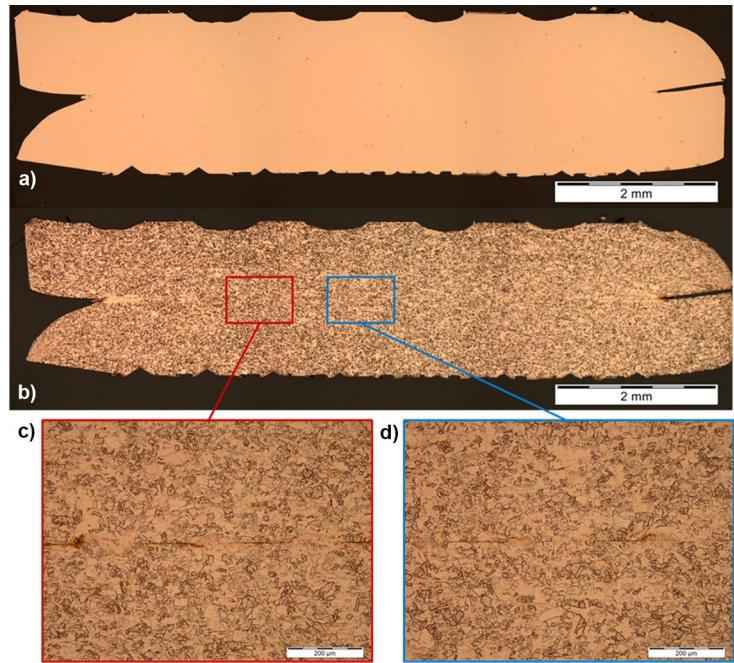
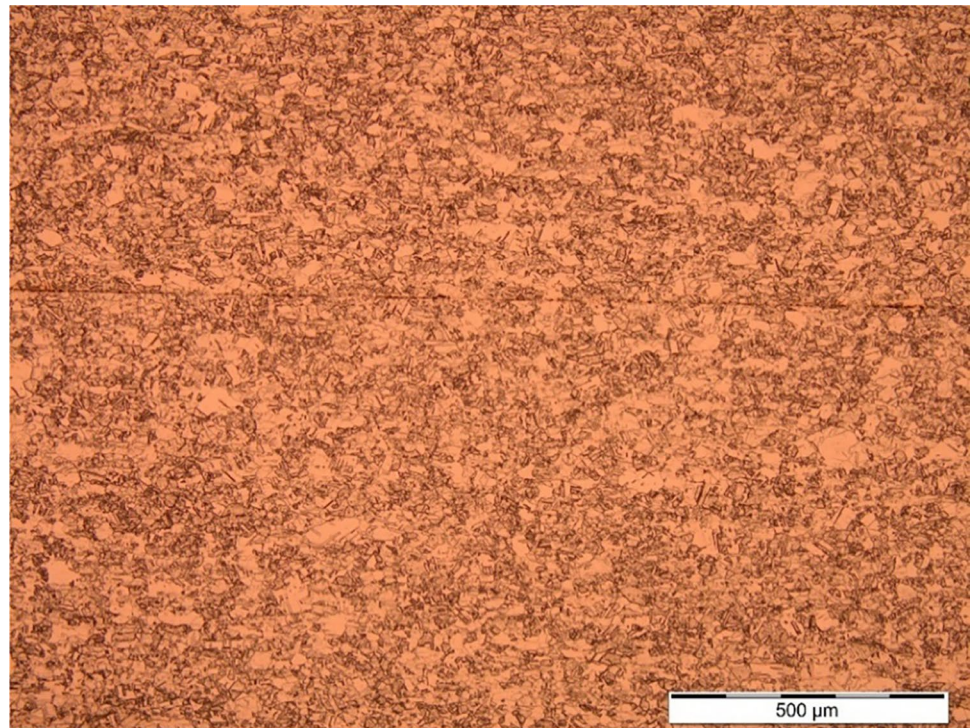


**Fig. 15** Interface of the sample prepared with sandpaper 180 mesh showing the phenomenon of a welded island in different areas of the weld

**Fig. 16** Detail ( $\times 100$ ) of the weld interface; sample prepared with sandpaper 500 mesh



The welded islands are larger for the rough milled samples than for the finish milled samples. This is a similar result as found for the sanded welds; a slightly roughened surface improves the amount of bonding between the workpieces. When the roughness decreases by using a finer sandpaper or mill, the friction between the workpieces decreases and this results in smaller welded islands. The Ra value obtained after rough milling is slightly larger than this obtained when using a sandpaper preparation with a 500 mesh, corresponding to larger peaks at the surface. The welded islands in the rough milled weld are larger than those

of the weld sanded with a 500 mesh, again showing that a rougher surface gives rise to larger welded zones.

Finally, the etched workpieces result in a satisfactory joining between the sheets prepared by polishing (Fig. 20). Several small welded islands are dispersed across the weld interface of this weld as can be seen on the detailed images in Fig. 20b. These islands are of the same order of magnitude as the welded islands in the weld interfaces obtained using surface preparations resulting in a low surface roughness such as finish milling, sandpaper with a 500 mesh and cleaning with acetone (Fig. 14).

**Fig. 17** Samples prepared by grinding: **a** polished image ( $\times 50$ ); **b** etched details ( $\times 100$ )

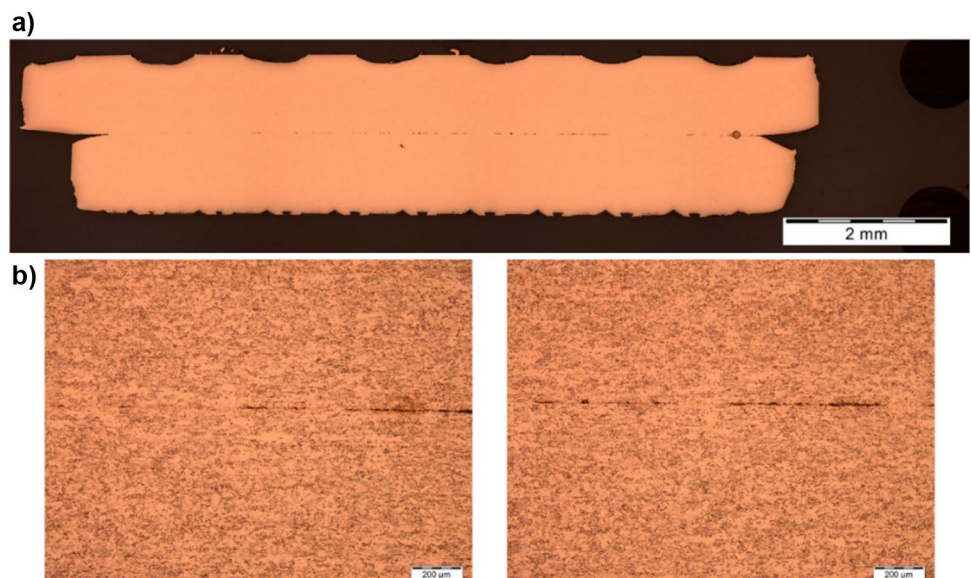


**Fig. 18** Sample prepared by rough milling: **a** polished image ( $\times 50$ ); **b** etched details ( $\times 200$ )

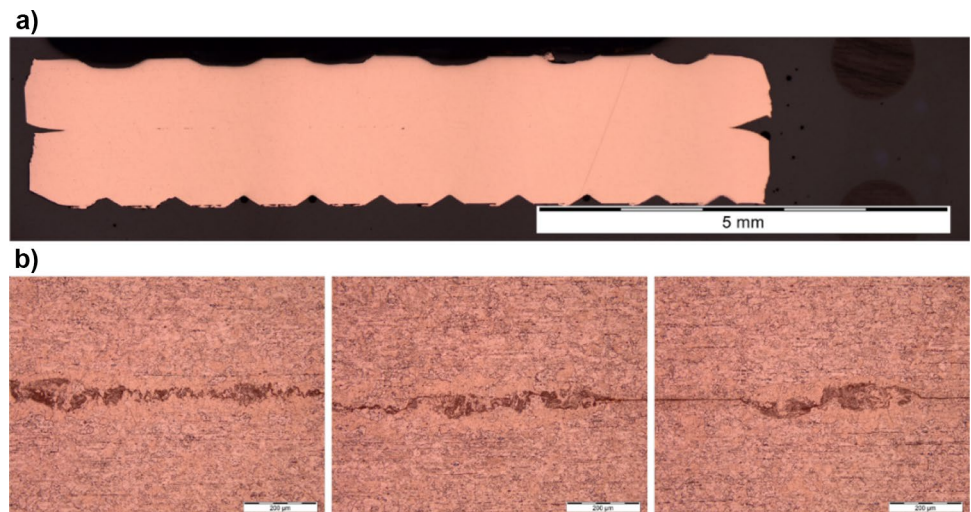


**Fig. 19** Sample prepared by finish milling: **a** polished image ( $\times 50$ ); **b** Etched details ( $\times 200$ )

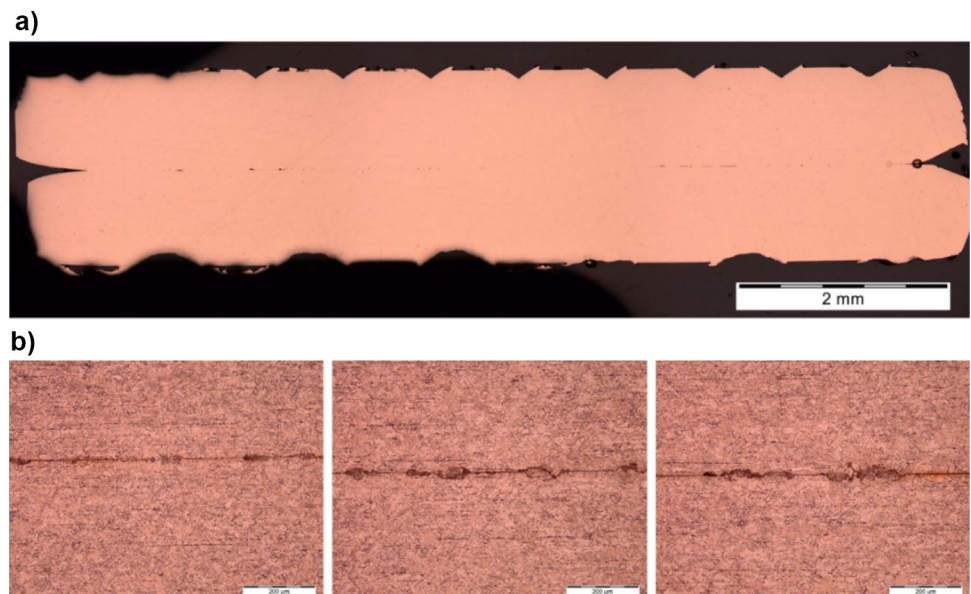
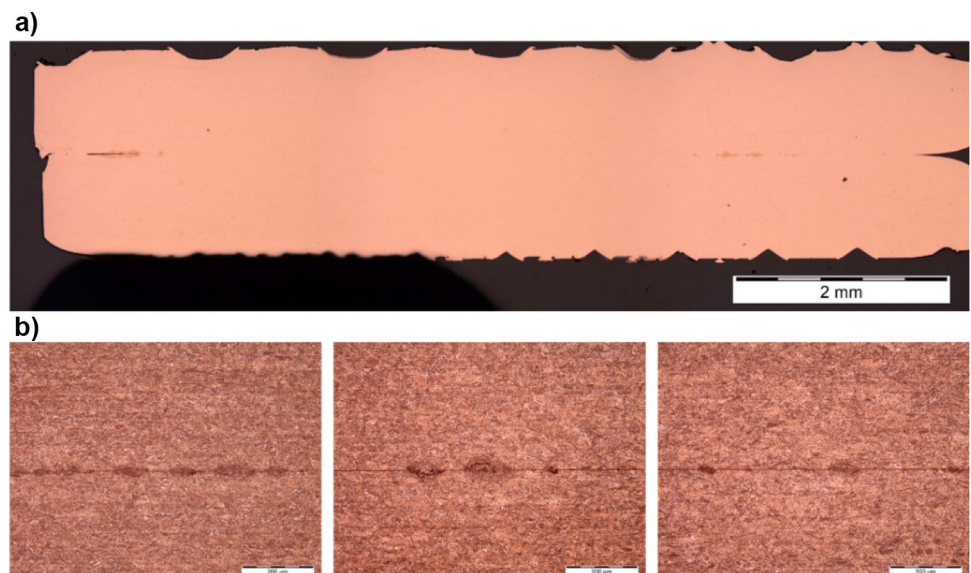


**Fig. 20** Samples prepared by polishing: **a** polished image ( $\times 50$ ); **b** etched details ( $\times 200$ )



## 4 Conclusions

This paper presents an effective strategy for determining the parameters of the ultrasonic welding process and determines the influence of basic parameters on the welding energy and the joint strength. Also the influence of various surface preparation methods on the joint properties was determined. The issue is currently of great importance, since ultrasonic welding is an effective method for joining metals used in electrical engineering, which may imply a growing interest in the ultrasonic welding technology, e.g. due to the development of electromobility. Based on the conducted experimental studies, a number of important observations were made and the conclusions listed below were drawn:

1. The ultrasonic vibration amplitude has the greatest impact on the strength of the joint.
2. The welding time has the greatest impact on the welding energy, and additionally, the welding time affects the amount of heat generated during the process. A too long welding time leads to excessive heating of the joined sheets, which results in a low-quality joint, characterized by a low strength.
3. A high surface roughness will result in mechanical interlocking and micro-welding of the surface asperities. On the other hand, a very low surface roughness will not cause enough friction between the sheets to create a joint.
4. The highest welding energy and tensile strength was obtained with a simple cleaning with acetone, making any additional surface preparation unnecessary.

**Author contribution** Conceptualization: Rafael Nunes, Koen Faes; experiments: Rafael Nunes, Koen Faes, Sylvia De Meester; analysis of research results: Rafael Nunes, Koen Faes, Wim De Waele; writing—original draft preparation: Rafael Nunes, Koen Faes, Sylvia De Meester, Andrzej Kubit; writing—review and editing: Koen Faes, Sylvia De Meester, Wim De Waele, Andrzej Kubit. All authors read and approved the final manuscript.

**Availability of data and material** The raw/processed data required to reproduce these findings are not shared.

**Code availability** Not applicable (The authors used commercial software).

## Declarations

**Ethics approval** The authors declare the compliance with the ethical standards.

**Consent to participate** Not applicable.

**Consent for publication** Not applicable.

**Competing interests** The authors declare no competing interests.

**Open Access** This article is licensed under a Creative Commons Attribution 4.0 International License, which permits use, sharing, adaptation, distribution and reproduction in any medium or format, as long as you give appropriate credit to the original author(s) and the source, provide a link to the Creative Commons licence, and indicate if changes were made. The images or other third party material in this article are included in the article's Creative Commons licence, unless indicated otherwise in a credit line to the material. If material is not included in the article's Creative Commons licence and your intended use is not permitted by statutory regulation or exceeds the permitted use, you will need to obtain permission directly from the copyright holder. To view a copy of this licence, visit <http://creativecommons.org/licenses/by/4.0/>.

## References

1. Faria R, Moura P, Delgado J, de Almeida AT (2012) A sustainability assessment of electric vehicles as a personal mobility system. *Energy Convers Manag* 61:19–30
2. Das A, Li D, Williams D, Greenwood D (2018) Joining technologies for automotive battery systems manufacturing. *World Electr Veh J* 9:22
3. Wu X, Liu T, Cai W (2015) Microstructure, welding mechanism, and failure of Al/Cu ultrasonic welds. *J Manuf Process* 20:321–331
4. Haddadi F, Tsivoulas D (2016) Grain structure, texture and mechanical property evolution of automotive aluminium sheet during high power ultrasonic welding. *Mater Charact* 118:340–351
5. Matsuoka S-I, Imai H (2009) Direct welding of different metals used ultrasonic vibration. *J Mater Process Technol* 209:954–960
6. Patel VK, Bhole SD, Chen DL (2013) Ultrasonic spot welding of lightweight alloys. In *Proceedings of the 13th International Conference on Fracture*, Beijing, China, 16–21 June, vol. 1, pp 30–39
7. Pati PR, Das S, Satpathy MP, Routara BC, Sahoo SK, Bhuyan SK (2020) Ultrasonic spot welding of Al-Cu sheets: a comprehensive study. *Mater Today Proc* 33:5168–5173
8. Das A, Barai A, Masters I, Williams D (2019) Comparison of tab-to-busbar ultrasonic joints for electric vehicle Li-ion battery applications. *World Electr Veh J* 10:55
9. Lee SS, Kim TH, Hu SJ, Cai WW, Abell JA, Li J (2013) Characterization of joint quality in ultrasonic welding of battery tabs. *J Manuf Sci Eng* 135:021004
10. Haddadi F (2016) Microstructure reaction control of dissimilar automotive aluminium to galvanized steel sheets ultrasonic spot welding. *Mater Sci Eng A* 678:72–84
11. Dhara S, Das A (2020) Impact of ultrasonic welding on multi-layered Al-Cu joint for electric vehicle battery applications: a layer-wise microstructural analysis. *Mater Sci Eng A* 791:139795
12. Çam G, Kocak M, dos Santos JF (1999) Developments in laser welding of metallic materials and characterization of the joints. *Welding in the World* 43(2):13–26
13. Çam G, Ventzke V, dos Santos JF, Koçak M, Jennequin G, Gonthier-Maurin P (1999) Characterisation of electron beam welded aluminium alloys. *Sci Technol Weld Join* 4(5):317–323
14. Çam G, Koçak M (2007) Microstructural and mechanical characterization of electron beam welded Al-alloy 7020. *J Mater Sci* 42(17):7154–7161
15. Zhang CQ, Robson JD, Prangnell PN (2016) Dissimilar ultrasonic spot welding of aerospace aluminum alloy AA2139 to titanium alloy TiAl6V4. *J Mater Process Technol* 231:382–388
16. Zhao YY, Li D, Zhang YS (2013) Effect of welding energy on interface zone of Al-Cu ultrasonic welded joint. *Sci Technol Weld Join* 18:354–360

17. Harthoorn JL (2005) Ultrasonic metal welding. *New Dev Adv Weld* 1978:1–141
18. Ipekoglu G, Çam G (2019) Formation of weld defects in cold metal transfer arc welded 7075-T6 plates and its effect on joint performance. *IOP Conf. Series: Materials Science and Engineering*, Vol. 629, The 2nd International Conference on Material Strength and Applied Mechanics 27–30 May 2019, Kiev, Ukraine
19. Çam G, Javaheri V, Heidarzadeh A (2022) Advances in FSW and FSSW of dissimilar Al-alloy plates. *J Adhes Sci Technol*. <https://doi.org/10.1080/01694243.2022.2028073>
20. Çam G (2017) Prospects of producing aluminum parts by wire arc additive manufacturing (WAAM). *Mater Today: Proc* 62(Part 1):77–85
21. Satpathy MP, Sahoo S (2017) Mechanical performance and metallurgical characterization of ultrasonically welded dissimilar joints. *J Manuf Process* 25:443–451
22. Li H, Cao B (2019) Effects of welding pressure on high-power ultrasonic spot welding of Cu/Al dissimilar metals. *J Manuf Process* 46:194–203
23. Shakil M, Tariq NH, Ahmad M, Choudhary MA, Akhter JI, Babu SS (2014) Effect of ultrasonic welding parameters on microstructure and mechanical properties of dissimilar joints. *Mater Des* 55:263–273
24. Haddadi F, Abu-Farha F (2016) The effect of interface reaction on vibration evolution and performance of aluminium to steel high power ultrasonic spot joints. *Mater Des* 89:50–57
25. Prangnell P, Haddadi F, Chen YC (2011) Ultrasonic spot welding of aluminium to steel for automotive applications—microstructure and optimization. *Mater Sci Technol* 27:617–624
26. Annoni M, Carboni M (2011) Ultrasonic metal welding of AA 6022–T4 lap joints: part I—technological characterisation and static mechanical behaviour. *Sci Technol Weld Join* 16:107–115
27. Bakavos D, Prangnell P (2010) Mechanisms of joint and microstructure formation in high power ultrasonic spot welding 6111 aluminium automotive sheet. *Mater Sci Eng A* 527:6320–6334
28. Macwan A, Chen D (2016) Ultrasonic spot welding of rare-earth containing ZEK100 magnesium alloy to 5754 aluminum alloy. *Mater Sci Eng A* 666:139–148
29. Panteli A, Robson J, Brough I, Prangnell P (2012) The effect of high strain rate deformation on intermetallic reaction during ultrasonic welding aluminium to magnesium. *Mater Sci Eng A* 556:31–42
30. Ni Z, Zhao H, Mi P, Ye F (2016) Microstructure and mechanical performances of ultrasonic spot welded Al/Cu joints with Al 2219 alloy particle interlayer. *Mater Des* 92:779–786
31. Gencsoy HT, Adams JA, Shin S (1967) On some fundamental problems in ultrasonic welding of dissimilar metals: Gencsoy, HT, Adams, J.A. and Shin S. *Weld. J.* 46:145
32. Kong C, Soar R, Dickens P (2003) Characterisation of aluminium alloy 6061 for the ultrasonic consolidation process. *Mater Sci Eng A* 363:99–106
33. Hu SJ, Senkara J, Zhang H (1996) Performance characteristics of resistance spot welds in the automotive industry: a structural point of view. *Proc IBEC* 96:91–98 (1996)
34. Hetrick ET, Baer JR, Zhu W, Reatherford LV (2009) Ultrasonic metal welding process robustness in aluminum automotive body construction applications. *Weld J* 88:149
35. Macwan A, Patel V, Jiang X, Li C, Bhole S, Chen D (2014) Ultrasonic spot welding of Al/Mg/Al tri-layered clad sheets. *Mater Des* 62:344–351
36. Balasundaram R, Patel V, Bhole S, Chen D (2014) Effect of zinc interlayer on ultrasonic spot welded aluminum-to-copper joints. *Mater Sci Eng A* 607:277–286
37. Gorji NE, O'Connor R, Brabazon D (2019) XPS, SEM, AFM, and Nano-Indentation characterization for powder recycling within additive manufacturing process. *IOP Conf Ser Mater Sci Eng* 1182(1):012025. <https://doi.org/10.1088/1757-899X/1182/1/012025>
38. Standard No. EN ISO 14273 (2016) Resistance welding - Destructive testing of welds - Specimen dimensions and procedure for tensile shear testing resistance spot and embossed projection welds
39. Kumar JP (2018) Effect of temperature distribution in ultrasonically welded joints of copper wire and sheet used for electrical contacts. *Materials* 11:101
40. Silva RGN, De Meester S, Faes K, De Waele W (2022) Development and evaluation of the ultrasonic welding process for copper-aluminium dissimilar welding. *J Manuf Mater Process* 6:6
41. Parkhimovich NY, Yusupova NR, Nazarov AA (2020) Strength of copper joints obtained by ultrasonic welding using copper intermediate layers in different structure states. *Lett Mater* 10(3):322–327
42. Elangovan S, Prakasan K, Jaiganesh V (2010) Optimization of ultrasonic welding parameters for copper to copper joints using design of experiments. *Int J Adv Manuf Technol* 51:163–171

**Publisher's Note** Springer Nature remains neutral with regard to jurisdictional claims in published maps and institutional affiliations.